Biogeosciences Discuss., 8, 5379–5422, 2011
www.biogeosciences-discuss.net/8/5379/2011/
doi:10.5194/bgd-8-5379-2011

Biogeosciences Discussions

Seasonal and inter-annual variability of plankton chlorophyll and primary production in the Mediterranean Sea: a modelling approach

P. Lazzari[1], C. Solidoro[1], V. Ibello[1,2], S. Salon[1], A. Teruzzi[1], K. Béranger[3], S. Colella[4], and A. Crise[1]

[1]Istituto Nazionale di Oceanografia e di Geofisica Sperimentale – OGS, Trieste, Italy
[2]Institute of Marine Sciences, Middle East Technical University, Erdemli, Turkey
[3]École Nationale Supérieure de Techniques Avancées, ENSTA ParisTech, Palaiseau, France
[4]Centro Nazionale delle Ricerche, CNR ISAC UOS, Roma, Italy

Received: 3 May 2011 – Accepted: 23 May 2011 – Published: 1 June 2011

Correspondence to: P. Lazzari (plazzari@ogs.trieste.it)

Published by Copernicus Publications on behalf of the European Geosciences Union.

Abstract

This study presents a model of chlorophyll and primary production in the pelagic Mediterranean Sea. A 3-D-ecosystem model (OPATM-BFM) was adopted to explore specific system characteristics and quantify key biogeochemical variables covering a 6-yr period, from 1999 to 2004.

We show that, on a basin scale, the Mediterranean Sea is characterised by a high degree of spatial and temporal variability in terms of primary production and chlorophyll concentrations. On a spatial scale, important horizontal and vertical gradients have been observed. In particular, notable differences between surface net primary production variability and the corresponding vertically integrated production rates have been identified, suggesting that care must be taken when inferring productivity in such systems from satellite observations alone. The present study indicates that seasonal variability dominates inter-annual differences.

According to the simulations over a 6-yr period, the developed model correctly simulated the climatological features of deep chlorophyll maxima and chlorophyll west-east gradients, as well as the seasonal variability in the primary offshore regions that were studied. The integrated net primary production highlights north-south gradients that differ from surface net primary production gradients and illustrates the importance of adopting a spatial and temporal description to calculate basin-wide budgets and their variabilities. According to the model, the western Mediterranean, in particular the Alboran Sea, can be considered mesotrophic, whereas the eastern Mediterranean is oligotrophic.

Finally, specific simulations that were designed to explore the role of ecosystem boundary conditions were performed. The subsequent results show that the effects of atmospheric and terrestrial nutrient loads on the total integrated net primary production account for less than 5 % of the annual budget, whereas an increase of 30 % in the light extinction factor impacts primary production by approximately 10 %.

BGD

8, 5379–5422, 2011

1 Introduction

The qualitative and quantitative dynamics of biogeochemical properties in the open ocean are not well understood despite a growing awareness of their importance to ecosystem functioning and related goods and services on a planetary scale.

Monitoring programmes are currently widespread in coastal areas but seldom cover open ocean waters, and they are principally devoted to the measurement of physical variables. Remote sensing observations provide valuable knowledge but primarily at the sea surface level. Research cruises enable scientists to explore ocean interiors; however, these are limited to a few transects per year and often have inadequate sampling rates at seasonal or inter-annual time scales. Biogeochemical floats and gliders are not currently used in sustained observational programmes.

As a result, we have typically a reasonable understanding of physical property dynamics, which are much easier to measure using remote and automated data collection systems. Conversely, we have less information regarding nutrient, chlorophyll and dissolved oxygen concentrations, and, moreover, rather sparse data at the basin scale on plankton primary production and other critical biological rates.

In this context, numerical models can offer an important contribution to the understanding of ecosystem dynamics by providing a virtual representation of reality that can be perfectly sampled.

The use of validated models to reconstruct and explore the spatial and temporal dynamics of a property that cannot be readily measured at high frequency is already quite common in other fields, such as hydrology and is now being increasingly applied in global ocean studies as well (Sarmiento and Gruber, 2006; Follows et al., 2007; Le Quéré et al., 2010). This is relevant despite the fact that, in these cases, it may not be possible to use strictly validated models (Arhonditsis and Brett, 2004). In principle, by optimally merging theoretical knowledge that is coded into a model with available experimental observations, data assimilation would provide a more accurate representation of reality than could be obtained from observations or models alone; however,

BGD
8, 5379–5422, 2011

experimental observations are too sparse to properly constrain the model output, with the exception of remote sensing information.

In this article, we explore the spatial and temporal variability of chlorophyll concentrations and plankton primary production rates in the epipelagic open ocean waters of the Mediterranean Sea (MS hereafter) with a state-of-the-art numerical model that is constrained by satellite data. Model results provide useful information for developing a better understanding of MS trophodynamics and 3-D climatological descriptions of biogeochemical properties that could be useful as evidence-based support for regulations that are aimed at marine protection and conservation (such as the Marine Strategy Framework Directive) or as a comparison point for future studies and cross-site analyses.

This article is organised as follows. Section 2 presents the methods and emphasises the main features of the MS and the numerical model that was adopted in this study. Section 3 presents the general results concerning chlorophyll concentrations and the rates of net primary production (NPP hereafter) and includes data-model comparisons. Annual budgets and temporal variability are proposed and compared to other sources considering different sub-basins. In section 4, the discussion analyses the spatial and temporal variabilities of biogeochemical properties and attempts to classify the results in light of general conceptual schemes (i.e., Longhurst, 1995). We conclude with a summary of the primary findings of this study.

2 Methods

2.1 The Mediterranean Sea

The MS is the largest semi-enclosed basin in the world. The Strait of Sicily separates the western and eastern sub-basins, which are also latitudinally shifted, and each sub-basin can, in turn, be subdivided into several regional seas based on bathymetric and morphological considerations (Fig. 1). Physical processes create a dynamic and

BGD
8, 5379–5422, 2011

complex picture in which mesoscale, thermohaline and wind driven circulations interact at different scales, resulting in a dominant west to east surface transport over both MS sub-basins, which is partially compensated for by intermediate east to west transport (Pinardi and Masetti, 2000).

The MS has long been considered one of the most oligotrophic areas in the world, Azov (1991). Low primary production annual budgets have been estimated by several studies based on in situ measurements (i.e., Sournia, 1973; Robarts et al., 1996; Moutin and Raimbault, 2002). Ocean colour satellite analysis clearly indicates a decreasing west-east trophic gradient (Bosc et al., 2004; Volpe et al., 2007; Barale et al., 2008; D'Ortenzio and Ribera d'Alcalà, 2009), which has been confirmed by (sparse) in situ measurements (Turley et al., 2000). Model analysis has indicated that this gradient is created by the superposition of physical dynamic features and asymmetric distributions of nutrient sources and is maintained by biological pump activity (Crispi et al., 2001). Satellite estimations have also demonstrated an analogous meridional trophic gradient from the north to the south (Siokou-Frangou et al., 2010). These spatial patterns are reflected in the features of the deep chlorophyll maximum (DCM), which is a quasi-permanent structure, except during the winter mixing period and is characterised by a zonal gradient in terms of depth (shallower in the west and deeper in the east; Crispi et al., 1999; Siokou-Frangou et al., 2010). Despite its oligotrophic features, the MS maintains high levels of biodiversity (Bianchi and Morri, 2000; Coll et al., 2010) and some hot spots of high fishery production (Caddy et al., 1995).

The lack of spatial-temporal coverage of in situ measurements does not allow for a direct estimate of the annual budget and temporal variability of NPP, except for specific sites, such as the DYFAMED station (Marty and Chiavérini, 2002) and other LTER stations (Pugnetti et al., 2006). Therefore, present estimates of this property at the basin scale are based on extrapolations of the sparse data sets that are available (Sournia, 1973).

BGD
8, 5379–5422, 2011

2.2 The numerical model

In this paper, we estimated the spatial and temporal variabilities of NPP rates and chlorophyll concentrations based on the outputs of a transport-reaction model (OPATM-BFM hereafter). Its components are based on the OPA transport model (Foujols et al., 2000) and BFM model (Vichi et al., 2007): these two physical and biogeochemical modules were originally coupled in an operational tool for studying MS biogeochemistry (Lazzari et al., 2010) and are applied here, with several modifications, for multi-annual simulations.

The model solves a system of partial differential equations in which the equation for the concentration c_i evolution in time reads:

$$\frac{\partial c_i}{\partial t} = A + D^v + S + R, \quad (1)$$

where A represents the advection term, D^v the vertical diffusion term, S the sinking term for particulates and R the reaction term, which describes local biogeochemical transformations.

The spatial-temporal dynamics of the system are determined by defining initial conditions (i.e., a value for each model variable for every point in the model domain at the initial time) and the boundary conditions (i.e., constraints that are required to compute time courses for exchanges of matter between the MS and its surroundings, i.e., including the Strait of Gibraltar, the sea surface and terrestrial loads).

2.2.1 The transport terms

The physical dynamics that are coupled with biogeochemical processes are pre-computed by a high resolution ocean general circulation model (OGCM), wherein all of the associated transport terms (advection A, vertical diffusion D^v and sinking S, see Eq. (1)) are integrated offline by a modified version of the OPA tracer model, version 8.1, on parallel machines via the method of domain decomposition according to the

BGD
8, 5379–5422, 2011

equations that are presented in Appendix A. The physical forcings are computed with the MED16 model outputs (Béranger et al., 2005) based on the OPA model (Madec et al., 1998). The OGCM circulation model supplies temporal evolution fields of zonal, meridional and vertical current velocity; vertical eddy diffusivity; potential temperature; and salinity, in addition to surface data for solar shortwave irradiance and wind stress. The studied period (1999–2004) has been validated by Béranger et al. (2009, 2010) who showed that the MED16 model is able to reproduce winter convection events in the main areas of the MS.

The offline integration scheme implies that concentrations of biogeochemical properties (other than salt) do not significantly affect circulation, which is a reasonably safe assumption in the MS.

2.2.2 The biogeochemical reaction term

The biogeochemical model (corresponding to the reaction term R in Eq. (1)) is a modified version of the Biogeochemical Flux Model, BFM. This model describes dissolved and particulate organic and inorganic components as functions of temperature, salinity, irradiance level and other biogeochemical properties (Fig. 2). This model's complexity has been chosen considering the need to describe energy and material fluxes through both "classical food chain" and "microbial food web" pathways (Thingstad and Rassoulzadegan, 1995), and it takes into account co-occurring effects of multi-nutrient interactions. Both of these factors are very important in the MS, wherein microbial activity fuels the trophodynamics of a large part of the system for much of the year and both phosphorus and nitrogen can play limiting roles (Krom et al., 1991; Béthoux et al., 1998).

The model presently includes four phytoplankton functional types (corresponding to pools of diatoms, flagellates, picophytoplankton and dinoflagellates): carnivorous and omnivorous mesozooplankton, bacteria, heterotrophic nanoflagellates and microzooplankton. Each of these variables is described in terms of its carbon, phosphorus, nitrogen, and silicon compositions.

BGD
8, 5379–5422, 2011

A detailed description of a standard BFM parameterisation is given in Vichi et al. (2007). In the version adopted here, we modified the chlorophyll synthesis parameterisation because several tests have shown that surface chlorophyll and NPP levels in the MS oligotrophic areas were higher than those identified via SeaWiFS satellite estimations and in-situ primary production measurements. The introduction of a multi-nutrient (nitrogen and phosphorus) limitation in the chlorophyll synthesis equation has improved this situation. Furthermore, we have constrained the model dynamics with a satellite-based light extinction coefficient.

Following the formulation of Geider et al. (1996), the BFM parameterisation describes gross primary production (*gpp*) as a function of PAR, temperature, carbon quota in plankton cells (C), chlorophyll content per unit of carbon biomass (θ) and, for diatoms only, silicate concentration. At the same time, the chlorophyll synthesis rate was proportional to the carbon synthesis rate which, in turn, was limited by internal nitrogen quotas but not by phosphorus quotas.

This formulation implies (as our tests indicated) that, even if both phosphate and nitrate are depleted in the upper layers, the lack of phosphorus does not enhance the effects of nitrogen-limiting on the synthesis of carbon and chlorophyll, which are, therefore, easily overestimated by the traditional BFM model. Indeed, the experiments of Geider and co-authors have exclusively explored nitrogen-limiting conditions (Geider et al., 1996, 1997, 1998); hence, the direct effects of phosphorus depletion have not been parameterised. A natural extension of Geider's formulation is, therefore, to include both phosphorus and nitrogen limitation in the carbon synthesis kinetics. As proposed by Flynn (2001), phosphorus-limiting conditions can be simulated by including a multi-nutrient limitation rule (involving phosphorus and nitrogen). Therefore, for consistency with the BFM formulation, we used the Liebig rule.

The revised formulation reads as shown in Appendix B, and the complete list of parameters that were used in our experiments is reported in the Supplement.

BGD
8, 5379–5422, 2011

2.2.3 Constraining the model using satellite observations

Several test simulations have revealed that standard formulations for light extinction factors based on water absorption and plankton self-shading (Riley, 1975) do not adequately describe the observed light attenuation along the water column and the spatial differences in DCM depth between MS sub-basins. We have assumed that the water optical properties were not of the Yerlov "case I" type, owing to the presence of "yellow substances" (CDOM) that can increase the water's absorption coefficient (Morel and Gentili, 2009). Because the dynamics of such substances cannot be modelled, we used a light extinction coefficient (k) that was derived from satellite observations. As a consequence, we implicitly included, albeit empirically, the effects of all dissolved and particulate matter. As shown in Fig. 3, k is space- and time-dependent: higher values are observed during the winter in the western Mediterranean area. The light model that was used to evaluate the photosynthetic available irradiance $I(z)$ at different depths (z) is based on the Lambert-Beer approximation:

$$I(z) = I(z_o)e^{-k(x,y,t)z} \quad (2)$$

$$k(x,y,t) = k_{\text{sat}}(x,y,t), \quad (3)$$

where $I(z_0)$ is the irradiance at the surface level, and x, y and t are longitude, latitude and time, respectively. The light attenuation term (k) is derived from SeaWiFS data (k_{sat}) adopting the diffuse attenuation coefficient at 490 nm (K490). k_{sat} consists of seasonal climatological measurements over the 1998–2004 period, which were spatially interpolated onto the model grid with a 5-day temporal frequency.

2.2.4 The initial and boundary conditions in the numerical experiments

The nutrient pools (nitrate, phosphate, silicate) and dissolved oxygen for the BFM biogeochemical model were initialised using vertical profiles that were provided by a retrospective reanalysis that had been performed during the MFSTEP project using the

BGD
8, 5379–5422, 2011

MEDAR-MEDATLAS 2002 data set (Crise et al., 2003). The extracted data include dissolved oxygen measurements (from 1948 to 2002), nitrate (from 1987 to 2002), phosphate (from 1987 to 2002) and silicates (1987 to 2002).

A vertical nutrient profile was assigned to each of the eleven regions, as reported in Crise et al. (2003). The other biogeochemical state variables were homogeneously initialised in the photic layer (0–200 m) according to the standard BFM values and with lower values in the deeper layers. The initialisation values that were obtained in this manner can be used as annual means for the climatological data set. A smoothing algorithm was applied to manage the discontinuities between the different sub-domains.

A Newtonian dumping (D^N) term regulates the Atlantic buffer zone that is outside of the Strait of Gibraltar:

$$D^N = \frac{1}{\tau}\left(c_i^D - c_i^t\right) \tag{4}$$

where τ is the time scale of the relaxation, and the concentration c_i is relaxed to the seasonally varying value c_i^D, which is derived from climatological MEDAR-MEDATLAS data (phosphate, nitrate, silicate, dissolved oxygen).

Atmospheric deposition rates of inorganic nitrogen and phosphorus were set according to the synthesis proposed by Ribera d'Alcalà et al. (2003) and based on measurements of field data (Löye-Pilot et al., 1990; Guerzoni et al., 1999; Herut and Krom, 1996; Cornell et al., 1995; Bergametti et al., 1992). No distinction was made between dry and wet depositions, and all of the deposited nutrients were considered to be bioavailable. The deposition rates were taken as constant during the year, with different values for the western (580 Kt N yr^{-1} and 16 Kt P yr^{-1}, for nitrates and phosphates, respectively) and eastern sub-basins (558 Kt N yr^{-1} and 21 Kt P yr^{-1}), and they were calculated by averaging the "low" and "high" estimates reported by Ribera d'Alcalà et al. (2003).

Nutrient loadings from rivers and continuous coastal sources were set according to the reconstruction of the spatial and temporal water discharge variabilities that were conducted according to the method described by Ludwig et al. (2009), with total nitrate

BGD
8, 5379–5422, 2011

and phosphate inputs of 826 Kt N yr^{-1} and 25 Kt P yr^{-1}, respectively. This review is based on available field data for nutrient concentrations, climate parameters that have been available since the early 1960s, and on model results for areas that are not covered by the data. The nutrient discharge rates for the major rivers (Po, Rhone and Ebro) take into account seasonal variability on a monthly scale and are calculated on the basis of direct observations. All other inputs are treated as constants throughout the year due to a lack of associated data.

2.3 Experimental procedure

In this work we compare projections of three selected runs. These runs were all characterised by the same code configuration, forcing fields and initial conditions. The simulations covered the period from 1999 to 2004, and the output files were stored on disk as 10-day averages. The reference numerical experiment OPATM-BFM REF (Table 1, column 1) was used in the results section to compare the simulation outputs to other estimations. The second simulation was configured without atmospheric and terrestrial inputs (ATIs) to assess the impacts of these inputs. The third run was conducted to analyse the impact of increasing the extinction factor k by 0.01 m^{-1} (where 0.01 m^{-1} represents 30 % of the minimum value of k), given that the satellite algorithm tends to underestimate extinction factors in oligotrophic areas (Psarra et al., 2000).

3 Results

In this section, we present model results for NPP rates and chlorophyll concentrations. Surface and vertically integrated distributions, both at the basin and sub-basin scales, and their evolution over seasonal and inter-annual time scales are presented. The NPP results are then compared to available measurements. To further corroborate the model, in situ data and satellite estimates were compared to the corresponding model variables. Because their spatial and temporal resolutions are different, observed

BGD
8, 5379–5422, 2011

data and model results were compared using suitable aggregation methods. Shallow areas (depth < 200 m) and marginal seas were excluded from the statistics because the model was designed for pelagic areas.

3.1 Spatial and temporal chlorophyll variability

We computed chlorophyll concentrations climatological fields by averaging all of the outputs for the 1999–2004 period. The climatological spatial variability throughout the MS was presented considering variables distribution along four transects (Fig. 1) that had been chosen to provide a good representation of the chlorophyll vertical structure, as previously proposed by D'Ortenzio and Ribera d'Alcalà (2009).

In the Alboran Sea (Fig. 4a), the DCM was quite shallow, at an average depth of approximately 60 m, and the associated chlorophyll concentration was approximately 0.25 mg chla m^{-3}. The DCM was found at roughly the same depth from the Alboran Sea area up to the western part of the Algerian region (5° E, Fig. 4a T1). In the south Ionian Sea and the Levantine region, the DCM was observed to occur at a quite uniform depth of approximately 110 m with average chlorophyll concentrations of approximately 0.1 mg chla m^{-3}. The north-south transects, which cut across the Levantine and the western sub-basins (T2, T3 and T4 in Fig. 1), indicate a gradient with a shallower DCM in the northern reaches of the sea, wherein chlorophyll concentrations of approximately 0.15–0.25 mg chla m^{-3} were observed at a depth of 70 m in the western sub-basin (Fig. 4b, T2) and 0.10–0.15 mg chla m^{-3} were observed at a depth of 110 m in the Levantine region (Fig. 4b, T4). The DCM in the Ionian transect (T3, Fig. 4c) also follows a gradient with deeper values in the southern part.

Moreover, the west-east DCM gradient that was observed by Turley et al. (2000; see their Table 2) and Moutin and Raimbault (2002; see their Table 1) in the period between May and June is a strong climatological signature reproduced by the model.

BGD
8, 5379–5422, 2011

We compared the average seasonal cycle in the 1999–2004 period that was obtained with the model output in a 1° box around the DYFAMED station (green solid line, Fig. 5), the median that was computed in the NWM region (black lines, Fig. 5) and the monthly climatological chlorophyll values that were measured at the DYFAMED station throughout the 1990–1999 period (Marty and Chiavérini, 2002). The results indicate that the simulation successfully described the observed marked seasonal cycle, both qualitatively and in terms of the maximum peak concentrations. Specifically, the seasonal cycle was characterised by a late winter maximum (60 mg chla m^{-2}), with a significant decrease reaching minimum values in May and a second relative maximum in June; however, according to the model results, the chlorophyll maximum occurred in February, which is one month earlier than in the observations and corresponds to a one-month delay after the climatological maximum winter convection of February.

The chlorophyll seasonal cycle that was described above for the DYFAMED station is consistent with the general behaviour of the chlorophyll that was modelled in the NWM area in the model, wherein maximum dispersions were observed to occur between January and March (Fig. 5, black lines). These results tend to support the hypothesis of Marty and Chiavérini (2002), who argued that the chlorophyll seasonal cycle that has been observed at the DYFAMED station is representative of a larger area in which open ocean processes drive the biotic dynamics of the ecosystem.

At the basin scale, the temporal and spatial variabilities of surface chlorophyll concentrations that were simulated by the model are compared to satellite results because of the high coverage of the latter data source. In Fig. 6 (left), the modelled surface chlorophyll concentrations that were obtained by aggregating median values for three representative regions (ALB, NWM, LEV) are compared to SeaWiFS level 4 composites that were reprocessed using a regional algorithm (Volpe et al., 2007) and interpolated onto the model grid. The seasonal cycle is present in all of the regions, wherein maximum values can be observed during February or March and minimum values in summer. This is also the period when the largest relative underestimation by the model is observed with respect to the satellite data, which was typically lower than

BGD
8, 5379–5422, 2011

0.05 mg chla m^{-3}. In the NWM region in particular, a one-month shift in the chlorophyll maximum can be observed. The spatial dispersions (25 and 75 percentiles) around the median value appear to be quite similar between the model and satellite data, as already observed in Lazzari et al. (2010) in the operational framework.

The model skill in each region can be graphically summarised with a target diagram (Jolliff et al., 2009). This diagram (Fig. 6, right) reports on the x-axis the unbiased root mean square difference (RMSD') between model results and reference data, whereas the y-axis indicates the bias (B') with respect to the reference data (in this case satellite). Both axes are normalised based on the variance of the satellite data. We computed B' and RMSD' for the climatological evolution of each grid cell of the model with respect to the reference satellite grid cell (interpolated onto the model grid), and we collapsed each cloud of data by computing median values of B' and RMSD' for each region. Because RMSD' is intrinsically positive, the sign of the x-axis was used to indicate whether the model variance was higher ($x > 0$) or lower ($x < 0$) than the satellite variance. The model results and reference data perfectly agree for points that are plotted at the centre of the target. All of the western regions are inside of the unitary circle, which indicates sufficient congruence with respect to the reference. The eastern regions are outside of the unitary circle; however, in those areas, the absolute error is very low due to the marked oligotrophic regime.

For all regions, B' is lower than 1, whereas RMSD' is positive for all regions with the exception of the NWM and SWE regions, wherein the temporal variance of the model is lower than that of the reference.

3.2 Net primary production

Climatological maps of the model's NPP calculations (Fig. 7) during the 1999–2004 period reveal that the surface chlorophyll, surface net primary production and vertically integrated NPP (int-NPP hereafter) differ, even if all of these presented the macro signal of the west-east trophic gradient.

BGD
8, 5379–5422, 2011

The most productive pelagic areas, with respect to surface NPP, include the Alboran Sea and the Liguro-Provençal region, whereas the eastern Mediterranean (including the ION and LEV regions) is remarkably uniform, unlike the surface chlorophyll distributions in these reaches.

A different picture emerges after analysing the int-NPP data (integrated from the surface to sea floor). The int-NPP signal from the Alboran Sea intrudes into the Algerian region, which is consistent with the water mass propagation of Atlantic Ocean water (anti-estuarine circulation). The north-south gradient in the western basin is less evident than that for surface NPP, and a south-north gradient can be observed in the Levantine region. A relative maximum of int-NPP rates appears along the south-western Sicilian coast, which can be ascribed to the persistent wind-driven upwelling events that are observed in this area (Béranger et al., 2004). The effects of river loadings on int-NPP values are very weak.

Table 1 compares the annual int-NPP budgets for several regions (simulated period 1999–2004) to other modelling experiments, satellite estimations and in situ data. When data are present for specific periods, the model results have been extracted for the same periods so as to facilitate direct comparisons.

The reference simulation OPATM-BFM REF (Table 1) indicates that the average int-NPP value for the entire MS is $98 \pm 5\,\mathrm{gC\,m^{-2}\,yr^{-1}}$, which is slightly higher than the findings of Sournia (1973), who have reported an MS budget of approximately 80–$90\,\mathrm{gC\,m^{-2}\,yr^{-1}}$, with an in situ ^{14}C method. These values can also be compared to satellite estimates, which range between 90 (Colella, 2006) and $135\,\mathrm{gC\,m^{-2}\,yr^{-1}}$ (Bosc et al., 2004). Higher int-NPP values are found in the western sub-basin, $131 \pm 6\,\mathrm{gC\,m^{-2}\,yr^{-1}}$, whereas lower values, $76 \pm 5\,\mathrm{gC\,m^{-2}\,yr^{-1}}$, are found in the eastern sub-basin. Satellite models give values of 112 and $163\,\mathrm{gC\,m^{-2}\,yr^{-1}}$ in the western sub-basin (Colella (2006) and Bosc et al. (2004), respectively) and values of 76 and $121\,\mathrm{gC\,m^{-2}\,yr^{-1}}$ in the eastern sub-basin (Colella (2006) and Bosc et al. (2004), respectively). Crispi et al. (2002) used a 3-D model to estimate an int-NPP rate of $120\,\mathrm{gC\,m^{-2}\,yr^{-1}}$ for the western sub-basin and $56\,\mathrm{gC\,m^{-2}\,yr^{-1}}$ for the

BGD
8, 5379–5422, 2011

eastern sub-basin. Moutin and Raimbault (2002) have measured values in excess of 350 mgC m^{-2} d^{-1} in the western area and 150 to 450 mgC m^{-2} d^{-1} in the eastern basin (May–June 1996, Minos Cruise). OPATM-BFM estimations for the same period of the year are 430 ± 258 mgC m^{-2} d^{-1} and 200 ± 107 gC m^{-2} yr^{-1}, respectively. The range of seasonal cycle variability (Table 1, "OPATM-BFM REF" column, first number in parentheses) is higher in the model than for the satellite data.

In the Alboran Sea, which is known to be the most productive MS area (Siokou-Frangou et al., 2010), our model estimates a production rate of 274 ± 12 gC m^{-2} yr^{-1}. The observed data do not cover all of the seasons; however, a comparison can be made for November 2003, wherein Macías et al. (2009) reported primary production data that were characterised by high spatial variabilities (6–644 mgC m^{-2} d^{-1}), whereas the current model estimated values of 545 ±3 21 mgC m^{-2} d^{-1}.

The elevated production signal from the Alboran Sea propagates into the Algerian region, which generates a spatial gradient that marks the declining influence of the Gibraltar Strait dynamics. The simulated annual budgets for the SWW and SWE areas are 160 ± 8 and 118 ± 13 gC m^{-2} yr^{-1}, respectively. An analysis by Lohrenz et al. (1988) of the Algerian Current (western part) in May period reported values ranging from 299 to 1288 mgC m^{-2} d^{-1}, whereas the model averaged results over the SWW for May of 570 ± 233 mgC m^{-2} d^{-1}. Moutin and Raimbault (2002) reported an int-NPP rate for the SWE area that was in excess of 450 mgC m^{-2} d^{-1}, whereas the model results for the same period are 447 ± 164 mgC m^{-2} d^{-1}.

The gradient between int-NPP rates in the NWM (116 gC m^{-2} yr^{-1}) and SWE (118 gC m^{-2} yr^{-1}) regions is very small, which is contrary to the picture that emerges from the regions' surface properties. Experimental data also do not show a clear gradient in terms of int-NPP (Moutin and Raimbault, 2002; see their Fig. 1). Conan et al. (1998) estimated an int-NPP in the range of 140–150 gC m^{-2} $yr^{-1}$for the years of 1992–1993 (NWM region), whereas other ^{14}C measurements for the Catalan-Balearic region range from 1000 ± 1 mgC m^{-2} d^{-1} (March period, Moran and Estrada, 2001) to 211–249 mgC m^{-2} d^{-1} (October period, Granata et al., 2004). The DYFAMED

BGD
8, 5379–5422, 2011

station measurements presented highly variable int-NPP rates, ranging from 86–232 $gC\,m^{-2}\,yr^{-1}$ for the 1993–1999 period, with an average of 156 $gC\,m^{-2}\,yr^{-1}$ (Marty and Chiavérini, 2002). A high degree of seasonal variability was also obtained in a one-dimensional modelling study for the same area and in other sites across the MS (Allen et al., 2002).

The Tyrrhenian Sea has an intermediate NPP range, $92 \pm 5\,gC\,m^{-2}\,yr^{-1}$, whereas Moutin and Raimbault (2002) have estimated values between 350 and 450 $mgC\,m^{-2}\,d^{-1}$ during the period from May–June (Minos cruise, 1996). The most oligotrophic areas, the Ionian Sea and Levantine region, have been characterised as having very low int-NPP values, 77 ± 4 and $76 \pm 5\,gC\,m^{-2}\,yr^{-1}$, respectively. Napolitano et al. (2000) estimated higher int-NPP rates (97 $gC\,m^{-2}\,yr^{-1}$) for the Rhodes gyre area via a one-dimensional model. Between May and June, the REF simulation calculates an int-NPP of $189 \pm 99\,mgC\,m^{-2}\,d^{-1}$ for the Ionian Sea, which is within the range that has been measured by Moutin and Raimbault (2002). In the same region, our August int-NPP estimates of $159 \pm 68\,mgC\,m^{-2}\,d^{-1}$ are in fair agreement with the measured rates of $186 \pm 65\,mgC\,m^{-2}\,d^{-1}$ (Boldrin et al., 2002). Similar agreement holds for the Levantine region.

The temporal series of int-NPP values is shown in Fig. 8. All of the regions are characterised by a strong seasonal cycle. As shown in Table 1, the inter-annual variability of the annual budget of int-NPP (red lines in Fig. 8) is lower than that of the seasonal cycle (black lines in Fig. 8). In the ALB region, the maxima are spread across the period from January–June. The western and eastern regions primarily differ in the int-NPP declining phase: in the western regions, the int-NPP winter peak is sustained for a longer period than in the eastern reaches.

4 Discussion

Numerical simulations give a virtual representation of reality which can be sampled at high frequency in both space and time and, therefore, allow us to fully cover and

BGD
8, 5379–5422, 2011

quantify the spatial and temporal variabilities of the biogeochemical and physical characteristics of pelagic systems and within each of its regions.

According to our basin-scale simulation, the normalised, time-averaged inter-quartile range (IQR) around the median chlorophyll concentration was between 60 % (ALB) and 35 % (SWE) and typically of the order of 45 %, whereas the normalised IQR was between 60 % (ALB) and 45 % (SWE) and typically of the order of 52 % for the int-NPP. These significant ranges imply that single measurements can rarely provide accurate representations of regional biogeochemical conditions or of annual productivity budgets.

Similarly, for all of the investigated regions, the instantaneous spatial variability of the int-NPP can exceed a normalised IQR of 100 % at any given moment, which highlights the need of an appropriate spatial sampling frequency.

Satellite-derived information may provide important knowledge about sea surface biogeochemical characteristics; however, our simulations indicate that there is not a uniform correlation between surface productivity and integrated NPP throughout the MS (Fig. 9). Differences are particularly marked in the SWW region, whereas in the TYR, ION and LEV regions, they collapse into a linear dependence (the correlation coefficient for the LEV region is equal to 0.91). Therefore, our results suggest that care should be taken in inferring conclusions regarding ocean conditions from satellite information alone, and a suite of tools should be used in driving informed conservation policies.

As already pointed out, the west-east spatial gradient in surface chlorophyll concentrations is also present for NPP rates. This gradient highlights the inaccuracy of treating the MS as a uniform, oligotrophic sea and the necessity of accounting for internal differences and regional sea typologies, especially with respect to environmental legislation. Specifically, adopting the Nixon classification of trophic regimes (Nixon, 1995) our estimates indicate that, on average, the MS is oligotrophic (int-NPP $< 100\,\mathrm{gC\,m^{-2}\,yr^{-1}}$), the western MS, particularly the Alboran Sea area, is mesotrophic (int-NPP $\in$ [100,300] $\mathrm{gC\,m^{-2}\,yr^{-1}}$), whereas the eastern regions remain oligotrophic.

BGD
8, 5379–5422, 2011

In contrast to common perceptions, the SWW region appears to be more productive than the NWM region. This difference persists after removing shallow water areas (depth < 200 m) from the estimate and elucidates the importance of Atlantic Ocean water inflow and the peculiar dynamics of the Alboran Sea that propagate the high productivity signal eastward in the sub-surface layers.

Because the light extinction factor that is used in these calculations is characterised by substantial uncertainty, we performed a simulation to evaluate the impact of increasing the extinction factor (k) by 0.01 m^{-1} (around 30 % of the base value). This analysis demonstrates the sensitivity of the system to k and results in a reduction in int-NPP of approximately 10 $gC\,m^{-2}\,yr^{-1}$. Moreover, this test revealed that the belt-like pattern of higher int-NPP, which is evident in the south Ionian and south Levantine regions as depicted in Fig. 7, is sensitive to k because the higher int-NPP rates that are present in the eastern area disappear with a 30 % increase in k (image not shown).

The behaviours of the region-averaged properties (Fig. 10, panel a) demonstrate that the MS can be classified according to the "*subtropical nutrient-limited winter-spring production period*" paradigm (Longhurst, 1995). The seasonal cycle of primary producers is fuelled by the wind-driven deepening of the mixed layer depth (MLD) that occurs in winter and produces a nutrient enrichment of the euphotic layer. Two regions can be considered according to the west-east trophic gradient, the NWM and LEV. In the NWM region, the maximum int-NPP is nearly synchronised with respect to the maximum of the MLD (*sensu* D'Ortenzio et al., 2005), whereas the minimum int-NPP is progressively reached in late autumn (Fig. 10, panel b). In the LEV region, the primary production peak also follows the MLD maximum; however, the signal in surface chlorophyll accumulation is less marked than that in the western regions (Fig. 10, panel c). The synchronisation between the MLD peak and the occurrence of peak chlorophyll concentrations, as is evident in Fig. 10 panels a–c, apparently contrasts with the usual sequence of bloom evolution: mixing and enrichment of the euphotic layer, followed by phytoplankton blooms only after stratification is re-established, which is a sequence that is known as the Gran effect (Mann and Lazier, 2006). Such an effect is important

BGD
8, 5379–5422, 2011

only when the MLD is deeper than the algal critical depth, which is reached when the total respiration rate along the water column is higher than the production rate. This occurs only in specific areas, whereas, on average, the production rate is higher than respiration rate during the mixing peak. The phytoplankton bloom for a grid point in a deep convection cell that is located in the NWM region (5.0625° E–42.1258° N; Fig. 10, panel d) mimics the Gran effect: in the case shown, the MLD is very deep (1500 m), and the increase in int-NPP and chlorophyll concentration occurs after the mixing peak is reached. Moreover, the deep mixing grid point reveals a higher bloom intensity and also a different timing of the bloom peak, which occurs one month later than the mean in the NWM region. In particular a too shallow MLD in the modelling framework could be at the base of the model chlorophyll maximum peak anticipation with respect to the DYFAMED station measurements.

The seasonal variability (second number in parentheses, Table 1) is higher in the model results than in the satellite data. Such variability agrees with the strong seasonal signal at the DYFAMED site (Marty and Chiavérini, 2002) and with the time series that was measured by Psarra et al. (2000) in the eastern MS. The temporal variability of int-NPP also qualitatively agrees with the time series of short wave radiation and wind speed (images not shown); in fact, for both forcings, the seasonal cycle is the strongest component of the signal, whereas the variability of the annual average is very low. The same arguments are valid for the variability of the mixed layer depth.

A comparison between different simulations (Table 2), which was performed with varying ATIs, indicates that the impact of these sources on the annual int-NPP budget amounts to an increase of $3\,\mathrm{gC\,m^{-2}\,yr^{-1}}$ and varies across different sub-basins over a range of $3–5\,\mathrm{gC\,m^{-2}\,yr^{-1}}$. These values are low in terms of total int-NPP rates but could be relevant with respect to the levels of new production.

BGD
8, 5379–5422, 2011

5 Conclusions

A model based synthesis of the chlorophyll concentrations and net primary production rates in the Mediterranean Sea for the 1999–2004 period is proposed in this work. Model simulations illustrate the high spatial and temporal variabilities of chlorophyll concentrations and integrated NPP rates and highlight the importance of considering these variables when performing basin-wide budgets and exploring basin-wide temporal variability.

According to the results obtained, the following summary points can be concluded:

- The model outcomes agree fairly well with prior in situ observations.
- The seasonal cycle signal of the integrated NPP dominates over the inter-annual variability when large scale averages are considered.
- The horizontal averages over selected regions show a clear trophic spatial gradient that decreases from west to east.
- The north-south patterns are different with respect to surface and integrated properties.
- The model results are in line with the Longhurst biological domain "*subtropical nutrient-limited winter-spring production period*".
- The impact of atmospheric and terrestrial inputs on the annual budget of the integrated NPP (new production) is in the range of 3–5 $gC\,m^{-2}\,yr^{-1}$.
- Moreover, the impact of a 30 % increase in the extinction factor (k) on the integrated NPP annual budget is approximately 10 $gC\,m^{-2}\,yr^{-1}$.

BGD
8, 5379–5422, 2011

Appendix A

Transport equations formulation

The ocean 3-D fields from the MED16 model at 1/16° resolution are horizontally interpolated on a 1/8° resolution grid taking care of the variable conservation while the original vertical grid is kept. In more details, the working meshgrid is based on 1/8° longitudinal scale factors (e_1) and on $1/8^\circ\cos(\varphi)$ latitudinal scale factor (e_2). The vertical meshgrid (e_3) accounts for 43 vertical z-levels: 13 in the first 200 m depth, 18 between 200 and 2000 m, 12 below 2000 m.

The temporal scheme is esplicit forward time scheme for the advection term (A) whereas an implicit time step is adopted for the vertical diffusion (D^v), with a time step of 1800s.

In numerical terms, the transport reaction equations are:

$$A = \left[\frac{1}{e_1 e_2 e_3} \left(\frac{\Delta\left(e_2 e_3 c_i^t u\right)}{\Delta i} + \frac{\Delta\left(e_1 e_3 c_i^t v\right)}{\Delta j} + \frac{\Delta\left(e_1 e_2 c_i^t w\right)}{\Delta k} \right) \right] \tag{A1}$$

The advection term A corresponds to the budget of all the fluxes across the boundaries of the cell with index (i longitude, j latitude, k depth) normalized on the cell volume ($e_1 e_2 e_3$).

$$D^v = \left[\frac{1}{e_3} \left(\frac{\Delta}{\Delta k} \left(\frac{k_v}{e_3} \frac{\Delta\left(c_i^{t+1}\right)}{\Delta k} \right) \right) \right] \tag{A2}$$

where k_v is the vertical eddy diffusivity coefficient and c_i are the concentration at time $t+1$.

The vertical diffusion term (D^v) is calculated by an implicit forward time scheme to increase the stability, especially in the vertical mixing phase where vertical diffusion

BGD
8, 5379–5422, 2011

coefficient can be very high.

The sinking term S is a vertical flux:

$$S = \left[\frac{1}{e_1 e_2 e_3} \left(\frac{\Delta \left(e_1 e_2 c_i^t w_s \right)}{\Delta k} \right) \right] \quad \text{(A3)}$$

where w_s is the sinking velocity that is fixed for particulate matter and dependent on nutrient for diatoms and dinoflagellates.

Appendix B

Photosynthesis formulation

The carbon (C) fixation, Eq. (B1) and chlorophyll (chl) synthesis, Eq. (B2), read:

$$\frac{\partial C}{\partial t} = \text{gpp} - \text{rsp} - \text{exu} - \text{pred}_\text{C} \quad \text{(B1)}$$

$$\frac{\partial chl}{\partial t} = f_P^{n,p} \rho_{chl} (\text{gpp} - \text{rsp} - \text{exu}) - t_\text{rate}\, chl + chl_\text{REL} - \text{pred}_{chl} \quad \text{(B2)}$$

in particular the gross productivity rate is defined as

$$\text{gpp} = p_m^\text{C} f^\text{E} f^\text{T} f^\text{S} C \quad \text{(B3)}$$

where P_m^C is the maximum potential uptake, f^T, f^S are the limitations for temperature and silicates (diatoms only), f^E, Eq. (B3), is the limiting factor for photosynthetic available radiation $I(z)$.

$$f^\text{E} = \left(1 - e^{-\frac{\alpha^{chl}(P) I(z) \theta}{P_m^\text{C}}} \right) \quad \text{(B4)}$$

BGD
8, 5379–5422, 2011

$$t_{\text{rate}} = \max(p_{\text{sdchl}}(P)(1 - f_{\text{P}}^{n,p}), 0) \tag{B5}$$

$$Chl_{\text{REL}} = \min(0, \text{gpp} - \text{rsp}) \max(Chl - p_{\text{qchlc}}(P)C, 0) \tag{B6}$$

ρ_{chl} is the rate of chlorophyll synthesis for unit of carbon fixation that regulates the degree of adaptation, expressed by the quota of chlorophyll over carbon θ, to the different light regimes. t_{rate} is the turnover rate based on nutrient stress and Chl_{REL} is a relaxation term toward optimal chlorophyll to carbon ratio ($p_{\text{qchlc}}(P)$). f^n and f^p are linear limitation terms, bounded between p_o and 1, based on nutrient to Carbon quota.

$$f^n \longrightarrow f^{n,p} = \min(f^n, f^p) \tag{B7}$$

$$f^n = L_{p_o,1}\left(\frac{Q_{\text{NC}}(P) - p_{\text{qnlc}}}{p_{\text{qnRc}}(P) - p_{\text{qnlc}}}\right), \quad f^p = L_{p_o,1}\left(\frac{Q_{\text{PC}}(P) - p_{\text{qplc}}(P)}{p_{\text{qpRc}}(P) - p_{\text{qplc}}(P)}\right) \tag{B8}$$

We switched from f^n to $f^{n,p}$ in order to represent phosphorus limitation. A full detailed description of all the biogeochemical model equations and correspondent parameters are included in the Supplement.

Supplementary material related to this article is available online at: http://www.biogeosciences-discuss.net/8/5379/2011/bgd-8-5379-2011-supplement.pdf.

Acknowledgements. This work was partially funded by projects V.E.C.T.O.R. (VulnErabilità delle Coste e degli ecosistemi marini italiani ai cambiamenti climaTici e loro ruolO nel ciclo del caRbonio mediterraneo; financed by Italian Special Research Fund FISR 2001), EC-FP6 SESAME-IP and Accordo di esecuzione tra CMCC ed OGS.

The simulations were carried out at the CINECA supercomputer centre (Bologna, Italy).

This work was granted access to the HPC resources of IDRIS of CNRS under allocation 2008 (i2008010227) made by GENCI. Atmospheric forcing was provided by ECMWF.

Karine Béranger thanks the Mercator project for support to the MED16 work.

BGD
8, 5379–5422, 2011

References

Allen, J. I., Somerfield, P. J., and Siddorn, J.: Primary and bacterial production in the Mediterranean Sea: a modelling study, J. Marine Syst., 33–34, 473–495, 2002.

Arhonditsis, G. B. and Brett, M. T.: Evaluation of the current state of mechanistic aquatic biogeochemical modelling, Mar. Ecol.-Prog. Ser., 271, 13–26, 2004.

Azov, I.: The Mediterranean Sea, a marine desert?, Mar. Pollut. Bull., 23, 225–232, 1991.

Barale, V., Jaquet, J.-M., and Ndiaye, M.: Algal blooming patterns and anomalies in the Mediterranean Sea as derived form SeaWiFS dataset (1998–2003), Remote Sens. Environ., 112, 3300–3313, 2008.

Béranger, K., Mortier, L., and Crépon, M.: Seasonal variability of water transport through the Straits of Gibraltar, Sicily and Corsica, derived from a high-resolution model of the Mediterranean circulation, Prog. Oceanogr., 66, 341–364, 2005.

Béranger, K., Mortier, L., Gasparini, G.-P., Gervasio, L., Astraldi, M., and Crépon, M.: The dynamics of the Sicily Strait: A comprehensive study from observations and models, Deep Sea Res. II, 51, 411–440, 2004.

Béranger, K., Testor, P., and Crépon, M.: Modelling water mass formation in the Gulf of Lion (Mediterranean Sea), WORKSHOP CIESM Monograph n°38 on Dynamics of Mediterranean deep waters, F. Briand Eds., Monaco, 2009.

Béranger, K., Drillet, Y., Houssais, M.-N., Testor, P., Bourdallé-Badie, R., Alhammoud, B., Bozec, A., Mortier, L., Bouruet-Aubertot, P., and Crépon, M.: Impact of the spatial distribution of the atmospheric forcing on water mass formation in the Mediterranean Sea, J. Geophys. Res., 115, C12041, doi:10.1029/2009JC005648, 2010.

Bergametti, G., Remoudaki, E., Losno, R., Steiner, E., and Chatenet, B.: Source, transport and deposition of atmospheric Phosphorus over the northwestern Mediterranean, J. Atmos. Chem., 14, 501–513, 1992.

Béthoux, J. P., Morin, P., Chaumery, C., Connan, O., Gentili, B., and Ruiz-Pino, D.: Nutrients in the Mediterranean Sea, mass balance and statistical analysis of concentrations with respect to environmental change, Mar. Chem., 63, 155–169, 1998.

Bianchi, C. N. and Morri, C.: Marine Biodiversity of the Mediterranean Sea: Situation, Problems and Prospects for Future Research, Mar. Pollut. Bull., 40(5), 367–376, 2000.

Boldrin, A., Miserocchi, S., Rabitti, S., Turchetto, M. M., Balboni, V., and Socal, G.: Particulate matter in the southern Adriatic and Ionian Sea: characterization and downward fluxes, J.

BGD
8, 5379–5422, 2011

Marine Syst., 33–34, 389–410, 2002.
Bosc, E., Bricaud, A., and Antoine, D.: Seasonal and interannual variability in algal biomass and primary production in the Mediterranean Sea, as derived from 4 years of SeaWiFS observations, Global Biogeochem. Cy., 18, GB1005, 2004.
Caddy, J. F., Refk, R., and Do-Chi, T.: Productivity estimates for the Mediterranean: evidence of accelerating ecological change, Ocean Coastal Manage., 26(1), 1–18, 1995.
Colella, S.: La produzione primaria nel Mar Mediterraneo da satellite: sviluppo di un modello regionale e sua applicazione ai dati SeaWiFS, MODIS e MERIS, Phd Thesis, Università "Parthenope" Napoli, 162 pp., 2006.
Coll, M., Piroddi, C., Steenbeek, J., Kaschner, K., Ben Rais Lasram, F., Aguzzi, J., Ballesteros, E., Bianchi, C. N., Corbera, J., Dailianis, T., Danovaro, R., Estrada, M., Froglia, C., Galil, B. S., Gasol, J. M., Gertwagen, R., Gil, J., Guilhaumon, F., Kesner-Reyes, K., Kitsos, M.-S., Koukouras, A., Lampadariou, N., Laxamana, E., López- F de la Cuadra, C. M., Lotze, H. K., Martin, D., Mouillot, D., Oro, D., Raicevich, S., Rius-Barile, J., Saiz- Salinas, J. I., San Vicente, C., Somot, S., Templado, J., Turon, X., Vafidis, D., Villanueva, R., and Voultsiadou, E.: The Biodiversity of the Mediterranean Sea: Estimates, Patterns, and Threats, PLoS One, 5(8), 1–34, 2010.
Conan, P., Pujo-Pay, M., Raimbault, M., and Leveau, M.: Hydrological and biological variability of the Gulf of Lions. II Productivity on the inner edge of the North Mediterranean Current, Oceanol, Acta, 21(6), 767–782, 1998.
Cornell, S., Rendell, A., and Jickells, T.: Atmospheric inputs of dissolved organic Nitrogen to the oceans, Nature, 376, 243–246, 1995.
Crise, A., Solidoro, C., and Tomini, I.: Preparation of initial conditions for the coupled model OGCM and initial parameters setting, MFSTEP report WP11, subtask 11310, 2003.
Crispi, G., Mosetti, R., Solidoro, C., and Crise, A.: Nutrient cycling in Mediterranean basins: the role of the biological pump in the trophic regime, Ecol. Model., 138, 101–114, 2001.
Crispi, G., Crise, A., and Solidoro, C.: Coupled Mediterranean ecomodel of the Phosphorus and Nitrogen cycles, J. Marine Syst., 33–34, 497–521, 2002.
Crispi. G., Crise, A., and Mauri, E.: A seasonal three-dimensional study of the nitrogen cycle in the Mediterranean Sea: Part II. Verification of the energy constrained trophic model, J. Marine Syst., 20, 357–379, 1999.
D'Ortenzio, F. and Ribera d'Alcalà, M.: On the trophic regimes of the Mediterranean Sea: a satellite analysis, Biogeosciences, 6, 139–148, doi:10.5194/bg-6-139-2009, 2009.

BGD
8, 5379–5422, 2011

D'Ortenzio, F., Iudicone, D., de Boyer Montegut, C., Testor, P., Antoine, D., Marullo, S., Santoleri, R., and Madec G.: Seasonal variability of the mixed layer depth in the Mediterranean Sea as derived from in situ profiles, Geophys. Res. Lett., 32, L12605, doi:doi:10.1029/2005GL022463, 2005.
Flynn, K. J.: A mechanistic model for describing dynamic multi-nutrient, light, temperature interactions in phytoplankton, J. Plankton Res., 23(9), 977–997, 2001.
Follows, M. J., Dutkiewicz, S., Grant, S., Chisholm, S. W.: Emergent Biogeography of Microbial Communities in a Model Ocean, Science, 315(5820), 1843–1846, 2007.
Foujols, M.-A., Lévy, M., Aumont, O., Madec, G.: OPA 8.1 Tracer Model Reference Manual. Institut Pierre Simon Laplace, 39 pp., 2000.
Geider, R. J., MacIntyre, H. L., and Kana, T. M.: Dynamic model of phytoplankton growth and acclimation: responses of the balanced growth rate and the chlorophyll a: Carbon ratio to light, nutrient-limitation and temperature, Mar. Ecol.-Prog. Ser., 148, 187–200, 1997.
Geider, R. J., MacIntyre, H. L., and Kana, T. M.: A dynamic model of photoadaptation in phytoplankton, Limnol. Oceanogr., 41(1), 1–15, 1996.
Geider, R. J., MacIntyre, H. L., and Kana, T. M.: A dynamic regulatory model of phytoplanktonic acclimation to light, nutrients, and temperature, Limnol. Oceanogr., 43(4), 679–694, 1998.
Granata, T. C., Estrada, M., Zika, U., and Merry, C.: Evidence for enhanced primary production resulting from relative vorticity induced upwelling in the Catalan Current, Sci. Mar., 68(1), 113–119, 2004.
Guerzoni, S., Chester, R., Dulac, F., Herut, B., Loÿe-Pilot, M.-D., Measures, C., Migon, C., Molinaroli, E., Moulin, C., Rossini, P., Saydam, C., Soudine, A., and Ziveri, P.: The role of atmospheric deposition in the biogeochemistry of the Mediterranean Sea. Prog. Oceanogr., 44(1–3), 147–190, 1999.
Herut, B. and Krom, M.: Atmospheric input of nutrients and dust to the SE Mediterranean, in The Impact of Desert Dust Across the Mediterranean, edited by: Guerzoni, S. and Chester, R., Kluwer Acad., Norwell, Mass., 349–358, 1996.
Jolliff, J. K., Kindle J. C., Shulman I., Penta, B., Friedrichs, M. A. M., Helber, R., Arnone R. A.: Summary diagrams for coupled hydrodynamic-ecosystem model skill assessment, J. Marine Syst., 76(1–2), 64–82, 2009.
Krom, M. D., Kress, N., Brenner, S., Gordon, L. I.: Phosphorus limitation of primary production in the eastern Mediterranean Sea, Limnol. Oceanogr., 36(3) 424–432, 1991.
Lazzari, P., Teruzzi, A., Salon, S., Campagna, S., Calonaci, C., Colella, S., Tonani, M., and

BGD
8, 5379–5422, 2011

Crise, A.: Pre-operational short-term forecasts for the Mediterranean Sea biogeochemistry, Ocean Sci., 6(1), 25–39, 2010.
Le Quéré, C., Takahashi, T., Buitenhuis, E. T., Rödenbeck, C., and Sutherland, S. C.: Impact of climate change and variability on the global oceanic sink of CO_2, Global Biogeochem. Cy., 24, GB4007 doi:10.1029/2009GB003599, 2010.
Löye-Pilot, M. D., Martin, J. M., and Morelli, J.: Atmospheric input of inorganic Nitrogen to the western Mediterranean, Biogeochem., 9, 117–134, 1990.
Lohrenz, S. E., Wiesenburg, D. A., DePalma, I. P., Johnson K. S., and Gustafson D. E.: Interrelationship among primary production, chlorophyll, and environmental conditions in frontal regions of the western Mediterranean Sea, Deep-Sea Res., 35(5), 793–810, 1988.
Longhurst, A. R.: Seasonal cycles of pelagic production and consumption, Prog. Oceanogr., 36(2), 77–167, 1995.
Ludwig, W., Dumont, E., Meybeck, M., and Heussner, S.: River discharges of water and nutrients to the Mediterranean and Black Sea: Major drivers for ecosystem changes during past and future decades?, Progr. Oceanogr., 80(3–4), 199–217, 2009.
Macías, D., Navarro, G., Bartual, A., Echevarría, F., and Huertas, I. E.: Primary production in the Strait of Gibraltar: Carbon fixation rates in relation to hydrodynamic and phytoplankton dynamics, Estuar. Coast. Shelf S., 83(2), 115–264, 2009.
Madec, G., Delecluse, P., Imbard, M., and Lévy, C.: OPA 8.1 Ocean General Circulation Model Reference Manual, Laboratoire d'Océanographie DYnamique et de Climatologie, Institut Pierre Simon Laplace, Paris, France, 91 pp., 1998.
Mann, K. H. and Lazier, J. R. N.: Dynamics of Marine Ecosystems. Blackwell Publishing, 496 pp., 2006.
Marty, J. C. and Chiavérini, J.: Seasonal and interannual variations in phytoplankton production at the DYFAMED time -series station (1991–1999), Deep-Sea Res. II, 49, 2017–2030, 2002.
Morán, X. A. G. and Estrada, M.: Short term variability of photosynthetic parameters and particulate abd dissolved primary production in the Alboran Sea (SW Mediterranean), Mar. Ecol.-Prog. Ser., 212, 53–67, 2001.
Morel, A. and Gentili, B.: The dissolved yellow substance and the shades of blue in the Mediterranean Sea, Biogeosciences, 6, 2625–2636, doi:10.5194/bg-6-2625-2009, 2009.
Morel, A. and Maritorena, S.: Bio-optical properties of oceanic waters: A reappraisal, J. Geophys. Res., 106(C4), 7163–7180, 2001.
Moutin, T. and Raimbault, P.: Primary production, Carbon export and nutrients availability in

BGD
8, 5379–5422, 2011

western and eastern Mediterranean Sea in early summer 1996 (MINOS cruise), J. Marine Syst., 33–34, 273–288, 2002.
Napolitano, E., Oguz, T., Malanotte-Rizzoli, P., Yilmaz, A., and Sansone, E.: Simulations of biological production in the Rhodes and Ionian basins of the eastern Mediterranean, J. Marine Syst., 24, 277–298, 2000.
Nixon, S. W.: Coastal marine eutrophication: a definition, social causes, and future concerns, Ophelia, 41, 199–219, 1995.
Pinardi, N. and Masetti, E.: Variability of the large scale general circulation of the Mediterranean Sea observations and modelling: a review, Palaeogeogr. Palaeocl., 158(3–4), 153–173, 2000.
Psarra, S., Tselepides, A., and Ignatiades, L.: Primary production in the oligotrophic Cretan Sea (NE Mediterranean): seasonal and interannual variability, Prog. Oceanogr., 46(2–4), 187–204, 2000.
Pugnetti, A., Camatti, E., Mangoni, O., Morabito, G., Oggioni, A., and Saggiomo, V.: Phytoplankton production in italian freshwater and marine ecosystems: state of the art and perspectives, Chem. Ecol., 22, (Supplement), S49–S69, 2006.
Ribera d'Alcalà, M., Civitarese, G., Conversano, F., and Lavezza, R.: Nutrient ratios and fluxes hint at overlooked processes in the Mediterranean Sea, J. Geophys. Res., 108(C9), 8106, doi:10.1029/2002JC001650, 2003.
Riley, G. A.: Transparency-chlorophyll relations, Limnol. Oceanogr., 20(1), 150–152, 1975.
Robarts, D. R., Zohary, T., Waiser, M. J., and Yacobi, Y. Z.: Bacterial abundance, biomass, and production in relation to phytoplankton biomass in the Levantine Basin of the southeastern Mediterranean Sea, Mar. Ecol.-Prog. Ser., 137, 273–281, 1996.
Sarmiento, J. L. and Gruber, N.: Ocean Biogeochemical Dynamics, PUP, 526 pp., 2006.
Siokou-Frangou, I., Christaki, U., Mazzocchi, M. G., Montresor, M., Ribera d'Alcalà, M., Vaqué, D., and Zingone, A.: Plankton in the open Mediterranean Sea: a review, Biogeosciences, 7, 1543–1586, doi:10.5194/bg-7-1543-2010, 2010.
Sournia, A.: La production primaire planctonique en Méditerraneée: Essai de mise à jour. Bull. Etude Commun. Méditer., 5, 1–128, 1973.
Thingstad, T. F. and Rassoulzadegan, F.: Nutrient limitations, microbial food webs, and "biological C-pumps": suggested interactions in a P-limited Mediterranean, Mar. Ecol.-Prog. Ser., 117, 299–306, 1995.
Turley, C. M., Bianchi, M., Christaki, U., Conan, P., Harris, J. R. W., Psarra, S., Ruddy, G.,

BGD
8, 5379–5422, 2011

Stutt, E. D., Tselepides, A., and Van Wambeke, F.: Relationship between primary producers and bacteria in oligotrophic sea: the Mediterranean and biogeochemical implication, Mar. Ecol.-Prog. Ser., 193, 11–18, 2000.

Vichi, M., Pinardi, N., and Masina, S.: A generalized model of pelagic biogeochemistry for the global ocean ecosystem, Part I: Theory, J. Marine Syst., 64, 89–109, 2007.

Volpe, G., Santoleri, R., Vellucci, V., Ribera d'Alcalà, M., Marullo, S., and D'Ortenzio, F.: The colour of the Mediterranean Sea: Global versus regional bio-optical algorithms evaluation and implication for satellite chlorophyll estimates, Remote Sens. Environ., 107, 625–638, 2007.

BGD

8, 5379–5422, 2011

Table 1. Horizontal averages of vertical integrated net primary productions (expressed in $gC\,m^{-2}\,yr^{-1}$ for climatology columns and in $mgC\,m^{-2}\,d^{-1}$ for the "specific periods" columns). In parentheses: in the model climatology columns (±/±) indicates the average of the annual variance/variance of the annual average; in the "specific period" model columns (±) indicates the variance. References: **(a)** Crispi et al. (2002), **(b)** Allen et al. (2002), **(c)** Napolitano et al. (2000), **(d)** Colella (2006), **(e)** Sournia et al. (1973), **(f)** Marty and Chiaverini (2002), **(g)** Boldrin et al. (2002), **(h)** Moutin and Raimbault (2002), **(i)** Macías et al. (2009), **(j)** Lohrenz et al. (2003), **(k)** Moran and Estrada (2001), **(l)** Granata et al. (2004), **(m)** Bosc et al. (2004), **(n)** Conan et al. (1998).

	Climatology/All seasonal cycle ($gC\,m^{-2}\,yr^{-1}$)					Specific periods ($mgC\,m^{-2}\,d^{-1}$)	
	OPATM-BFM REF	Other models	Satellite model[(d)]	Other satellite models	In situ	OPATM-BFM REF	In situ
Mediterranean (MED)	98 (±82/±5)	–	90 (±48/±3)	135[(m)]	80–90[(e)]	–	–
Western basin (WES)	131 (±98/±6)	120[(a)]	112 (±65/±7)	163[(m)]	–	430 (±258)	> 350[(h)] (May–Jun)
Eastern basin (EAS)	76 (±60/±5)	56[(a)]	76 (±20/±2)	121[(m)]	–	200 (±107)	150–450[(h)] (May–Jun)
Alboran Sea (ALB)	274 (±155/±11)	24–207[(b)]	179 (±116/±13)	–	–	545 (±321)	6–644[(i)] (Nov)
South West Med (SWW)	160 (±89/±8)	24–207[(b)]	113 (±43/±6)	–	–	570 (±233)	299–1288[(i)] (May)
South West Med (SWE)	118 (±70/±13)	–	102 (±38/±4)	–	–	447 (±164)	> 450[(h)] (May–Jun)
North West Med (NWM)	116 (±79/±6)	32–273[(b)]	115 (±67/±8)	–	86–232[(f)] 140–150[(n)]	600 (±290)/ 142 (±96)	1000±11[(k)](Mar)/ 211–249[(l)](Oct)
Tyrrhenian (TYR)	92 (±63/±5)	–	90 (±35/±7)	–	–	279 (±118)	350–450[(h)] (May–Jun)
Ionian (ION)	77 (±58/±4)	27–153[(b)]	79 (±23/±2)	–	62[(g)]	189 (±99)/ 159 (±68)	150–450[(h)] (May–Jun)/ 186±65[(g)] (Aug)
Levantine (LEV)	76 (±61/±5)	97[(c)]/ 36–158[(b)]	72 (±21/±2)	–	–	208 (±110)	150–250[(h)] (May–Jun)

BGD
8, 5379–5422, 2011

Table 2. Horizontal averages of vertical integrated net primary productions ($gC\,m^{-2}\,yr^{-1}$) for selected model simulations.

	OPATM-BFM REF	OPATM-BFM without ATI	OPATM-BFM REF (k+0.01)
Mediterranean (MED)	98 (±82/±5)	95 (±85/±4)	87 (±74/±7)
Western basin (WES)	131 (±98/±6)	127 (±103/±5)	120 (±89/±7)
Eastern basin (EAS)	76 (±60/±5)	73 (±61/±4)	64 (±53/±8)
Alboran Sea (ALB)	274 (±155/±11)	273 (±129/±12)	243 (±137/±7)
South West Med (SWW)	160 (±89/±8)	156 (±91/±7)	145 (±79/±6)
South West Med (SWE)	118 (±70/±13)	113 (±71/±12)	109 (±66/±12)
North West Med (NWM)	116 (±79/±6)	111 (±84/±6)	108 (±75/±7)
Tyrrhenian (TYR)	92 (±63/±5)	88 (±66/±5)	88 (±62/±6)
Ionian (ION)	77 (±58/±4)	74 (±61/±3)	68 (±54/±6)
Levantine (LEV)	76 (±61/±5)	73 (±61/±6)	60 (±51/±11)

BGD
8, 5379–5422, 2011

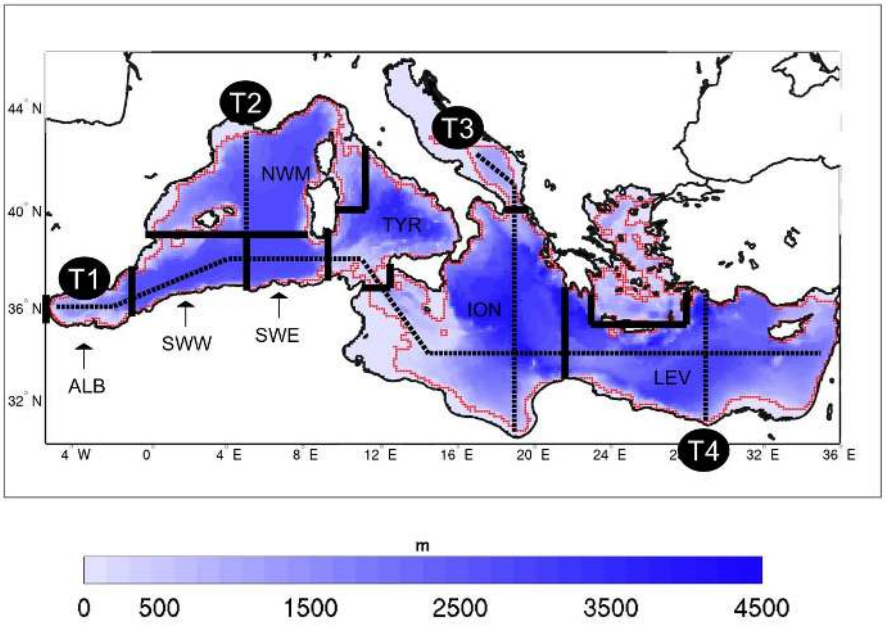

Fig. 1. Map of Mediterranean Sea bathymetry, with a-priori defined regions (delimited by solid black lines) and T1, T2, T3 and T4 transects (dashed black lines). Red line indicates shallow water limits (depth < 200 m).

BGD
8, 5379–5422, 2011

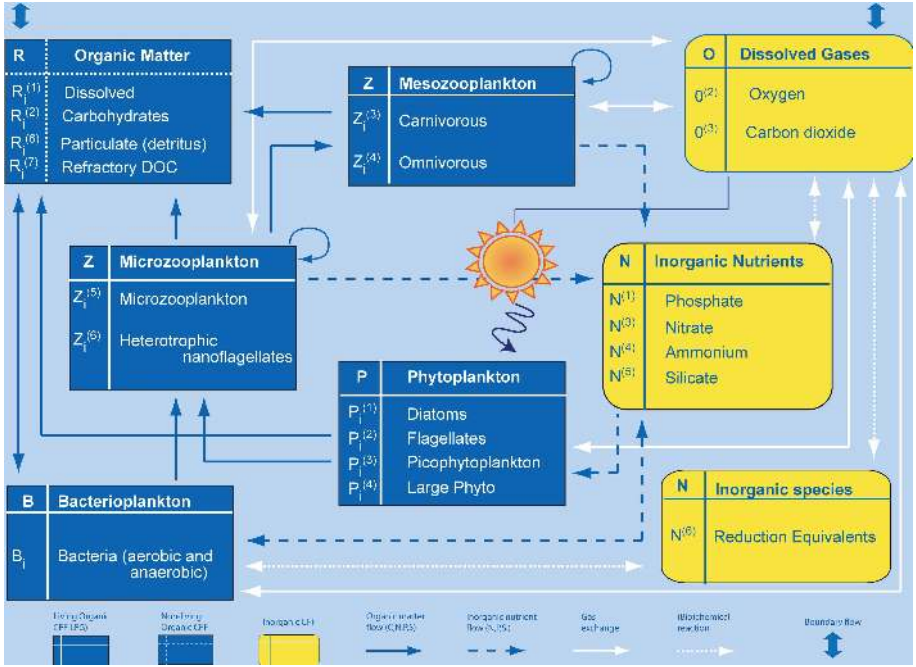

Fig. 2. Scheme of the BFM reactor.

BGD
8, 5379–5422, 2011

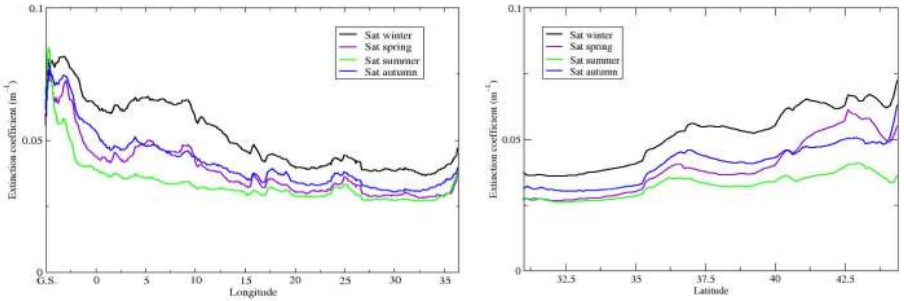

Fig. 3. Satellite extinction factor used in model simulations, zonal averages (left panel) and meridional averages (right panel), data provided by GOS-ISAC-CNR.

BGD
8, 5379–5422, 2011

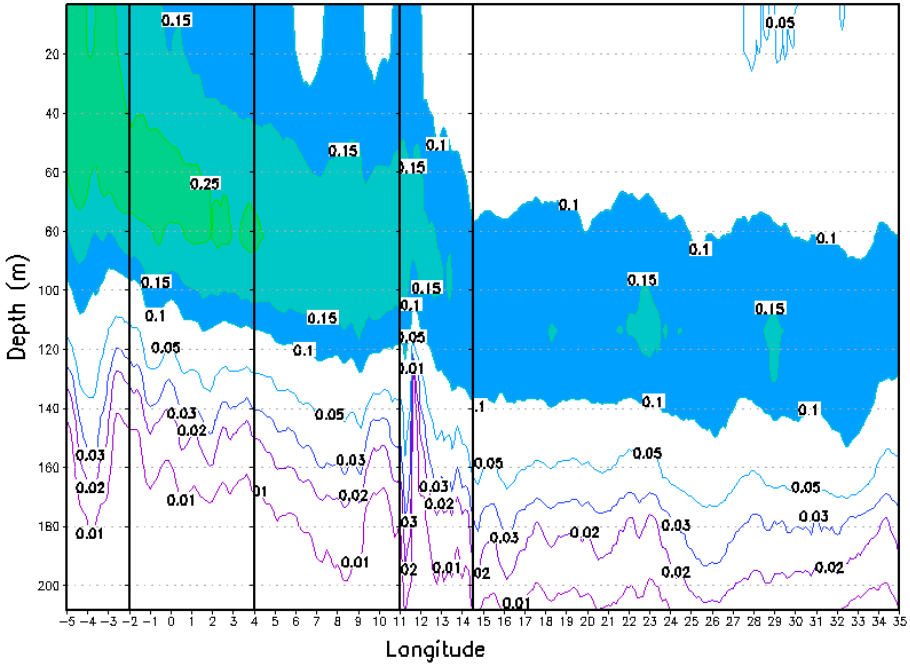

Fig. 4a. Vertical section of average chlorophyll (mg chla m^{-3}) along the T1 zonal transect (see Fig. 1) from OPATM-BFM REF run averaged for the period 1999–2004.

BGD
8, 5379–5422, 2011

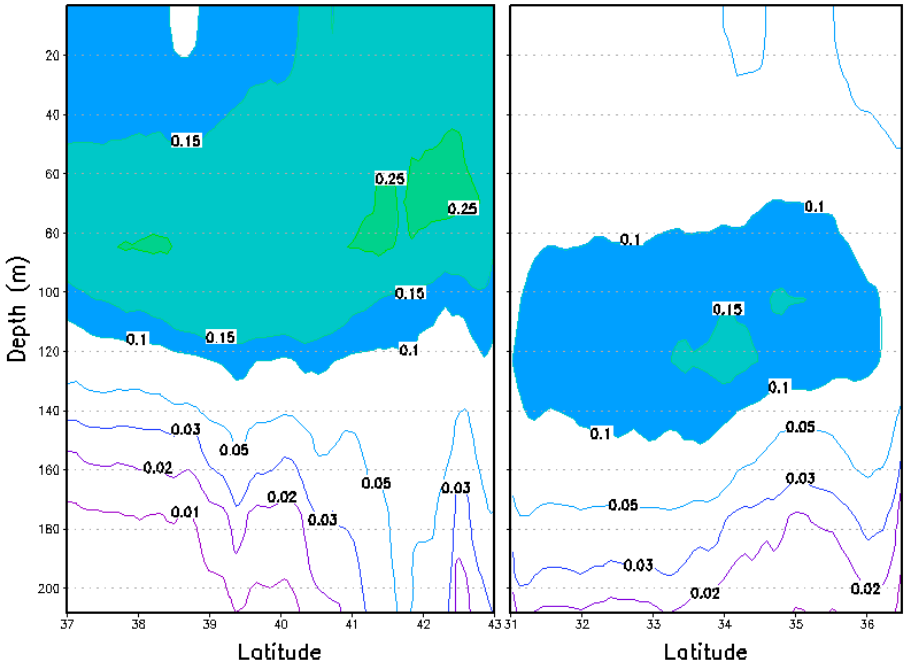

Fig. 4b. Vertical section of average chlorophyll (mg chla m^{-3}) from OPATM-BFM REF run along the T2 (left) and T4 (right) meridional transects (see Fig. 1) for the 6-yr period 1999–2004.

BGD
8, 5379–5422, 2011

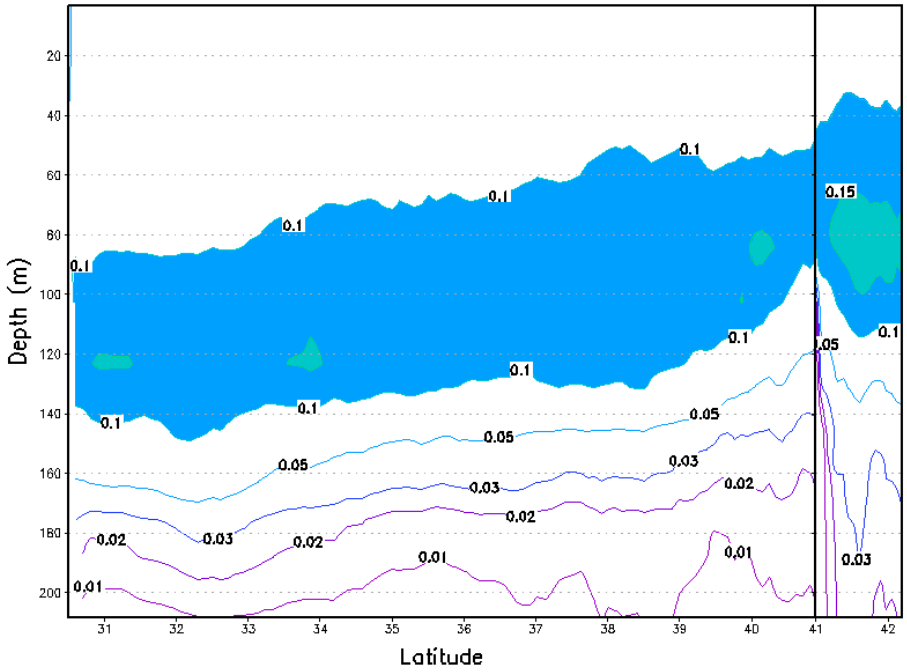

Fig. 4c. Vertical section of average chlorophyll (mg chla m^{-3}) from OPATM-BFM REF run along the T3 meridional transect (see Fig. 1) for the period 1999–2004.

BGD
8, 5379–5422, 2011

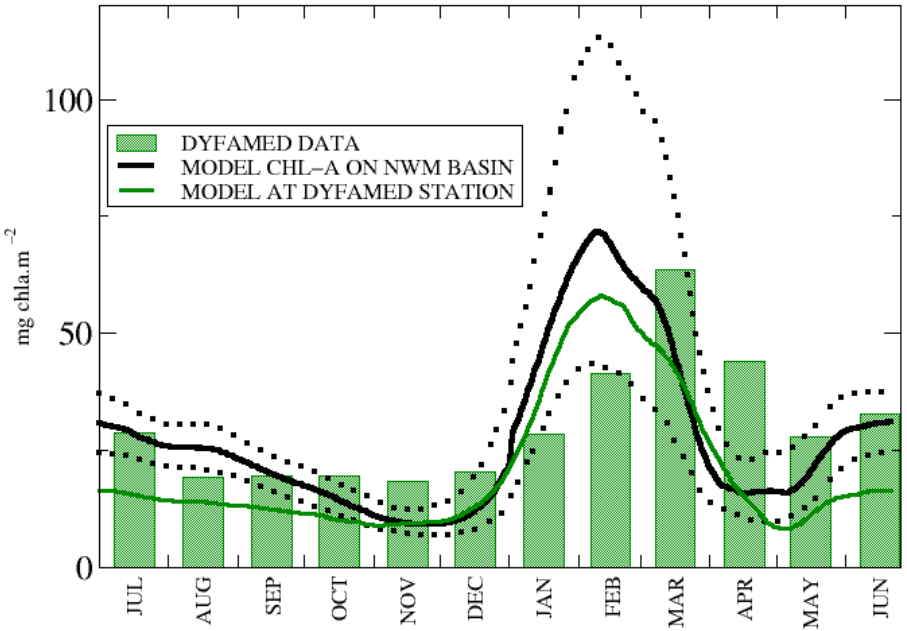

Fig. 5. Vertically integrated chlorophyll (mg chla m^{-2}). Climatological in situ data at the DYFAMED station are in green boxes (7.87° E, 43.42° N) for the period 1990–1999 (Marty and Chavièrini, 2002). Black lines represent average model results in the NWM region for the period 1999–2004 (solid median, dotted are 25 and 75 percentile). Green line is the average model results in a box (7.31–8.44° E, 42.86–43.95° N) around the DYFAMED station.

BGD
8, 5379–5422, 2011

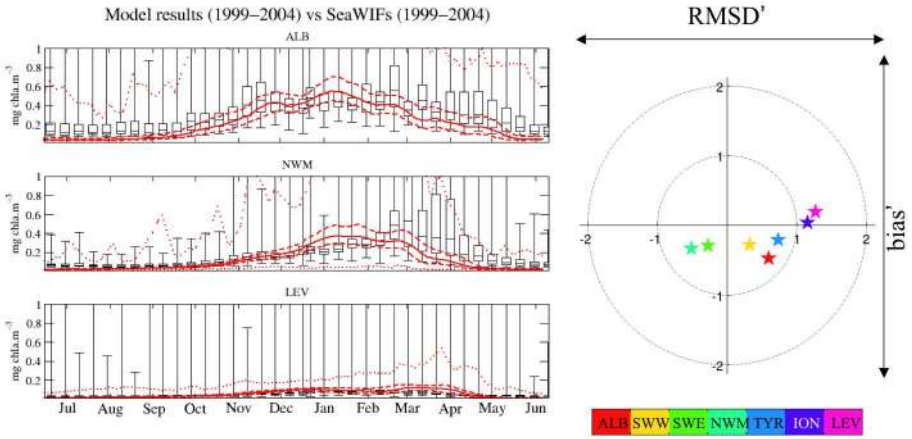

Fig. 6. Surface chlorophyll seasonal cycle (mg chla m^{-3}) for the period 1999–2004 simulated by OPATM-BFM model (solid red lines = median, dashed red lines = 25 and 75 percentile, dotted red lines = min and max) compared with the satellite SeaWIFs data set (box-plot). Data are spatially aggregated on three selected regions (ALB, NWM, LEV) using a spatial median. On the right panel the target diagram compares the model output chlorophyll seasonal cycle with SeaWIFs data seasonal cycle. Each star is the median of the temporal skill of each pixel for the specific region.

BGD
8, 5379–5422, 2011

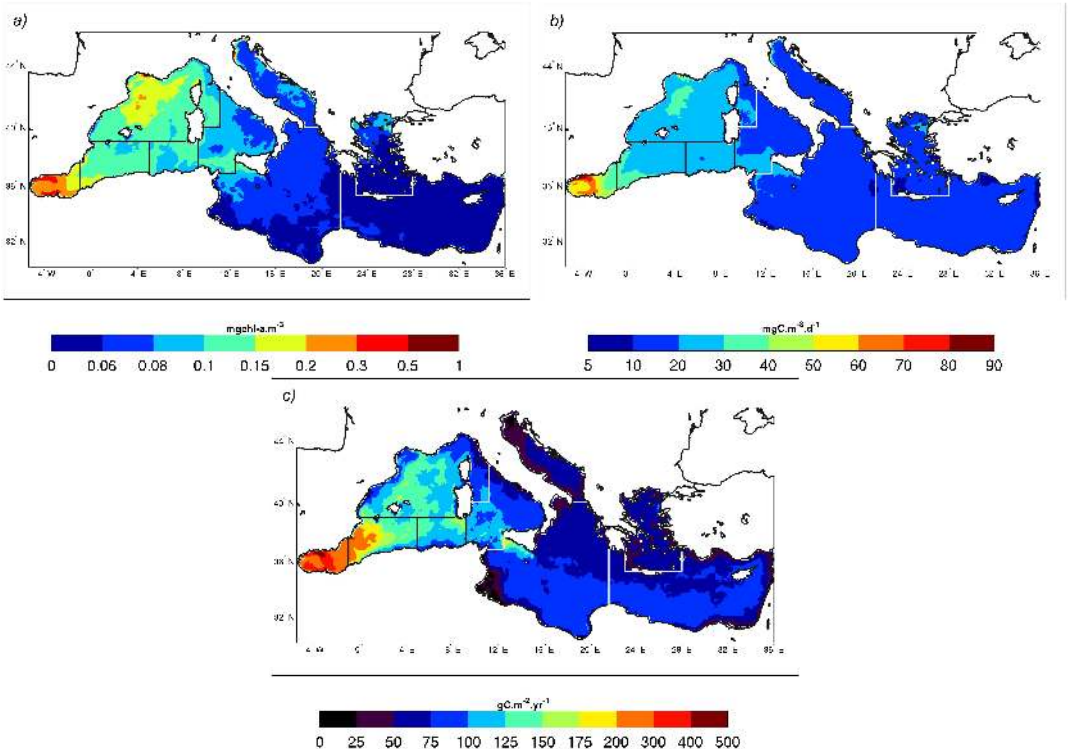

Fig. 7. Panel **(a)**: model climatology (period 1999–2004) of chlorophyll surface concentration (mg chla m^{-3}). Panel **(b)**: surface net primary production (mgC m^{-3} d^{-1}). Panel (c): vertically integrated net primary production (gC m^{-2} yr^{-1}).

BGD
8, 5379–5422, 2011

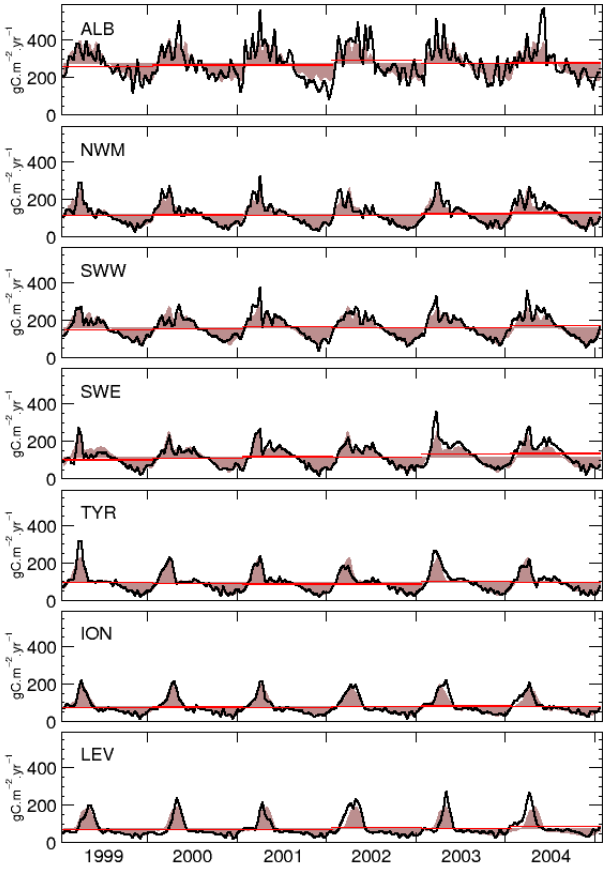

Fig. 8. Temporal series of integrated net primary production ($gC\,m^{-2}\,yr^{-1}$) averaged for the 7 areas of Fig. 1: ALB, NWM, SWW, SWE, TYR, ION, LEV (black line); climatological values for the period 1999–2004 (brown shading), and annual averages (red lines).

BGD
8, 5379–5422, 2011

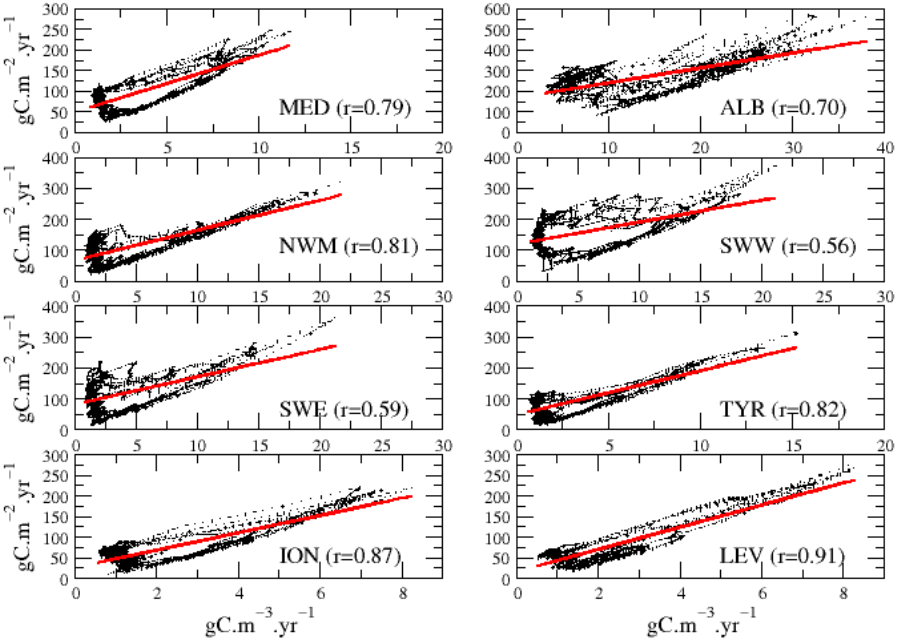

Fig. 9. Scatter plots of integrated ($gC\,m^{-2}\,yr^{-1}$) versus surface ($gC\,m^{-3}\,yr^{-1}$) net primary production: each point represents the 10-day regional average in the period 1999–2004 for the MS and the 7 areas defined in Fig. 1. Red lines represent the linear regressions, the correlation coefficient *r* is reported in parentheses for each area.

BGD
8, 5379–5422, 2011

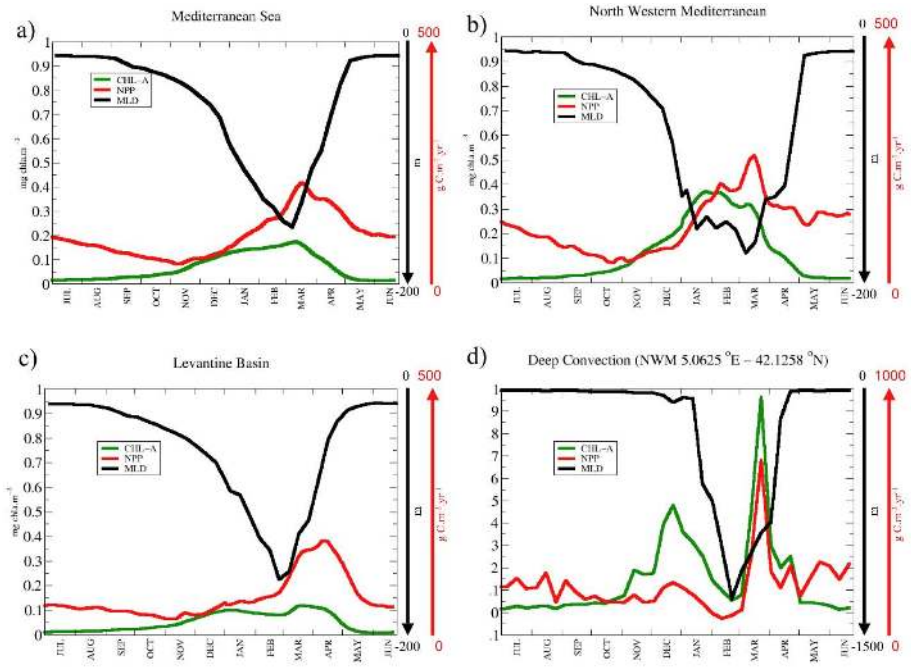

Fig. 10. Longhurst plots for MS **(a)**, NWM region **(b)**, LEV region **(c)** and deep convection grid point in the NWM **(d)**. Surface chlorophyll (chl-*a* in green) is expressed in mg chla m^{-3}, integrated net primary production (NPP in red) in gC m^{-2} yr^{-1}, mixed layer depth (MLD in black) in meters. Note the different scale for the NPP and MLD in panel **(d)**.

BGD
8, 5379–5422, 2011